Predictability of Explosive Cyclogenesis over the Northwestern Pacific Region Using Ensemble Reanalysis

AKIRA KUWANO-YOSHIDA

Earth Simulator Center, Japan Agency for Marine-Earth Science and Technology, Yokohama, Kanagawa, Japan

TAKESHI ENOMOTO

Disaster Prevention Research Institute, Kyoto University, Uji, Kyoto, Japan

(Manuscript received 1 June 2012, in final form 24 May 2013)

ABSTRACT

The predictability of explosive cyclones over the northwestern Pacific region is investigated using an ensemble reanalysis dataset. Explosive cyclones are categorized into two types according to whether the region of the most rapid development is in the Sea of Okhotsk or Sea of Japan (OJ) or in the northwestern Pacific Ocean (PO). Cyclone-relative composite analyses are performed for analysis increments (the differences between the analysis and the 6-h forecast) and ensemble spreads (the standard deviations of ensemble members of the analysis or first guess) at the time of the maximum deepening rate. The increment composite shows that the OJ explosive cyclone center is forecast too far north compared to the analyzed center, whereas the PO explosive cyclone is forecast shallower than the analyzed center. To understand the cause of these biases, a diagnosis of the increment using the Zwack–Okossi (Z-O) development equation is conducted. The results suggest that the increment characteristics of both the OJ and PO explosive cyclones are associated with the most important cyclone development mechanisms. The OJ explosive cyclone forecast error is related to a deeper upper trough, whereas the PO explosive cyclone error is related to weaker latent heat release in the model. A diagnosis of the spread utilizing the Z-O development equation clarifies the mechanism underlying the uncertainty in the modeled sea level pressure. For OJ explosive cyclones, the spread of adiabatic warming causes substantial sea level pressure spreading southwest of the center of the cyclones. For PO explosive cyclones, the latent heat release causes substantial sea level pressure spreading around the cyclone center.

1. Introduction

Explosive extratropical cyclones can cause violent winds, heavy rain/snow, and storm surges (Sanders and Gyakum 1980; Roebber 1984). Explosive cyclones are sometimes difficult to forecast (Sanders 1987; Gyakum et al. 1996). One reason for this difficulty is that explosive cyclogenesis results from a combination of several mechanisms that includes upper-level cyclonic vorticity advection, low-level warm air advection, and latent heat release (Shapiro et al. 1999). Uccellini et al. (1985) suggest the importance of an upstream trough that accompanied tropopause folding in the explosive cyclogenesis of the Presidents' Day Storm (1979). Chen and Dell'osso (1987) suggest the importance of latent heat release and the presence of a low-level jet for the development of an explosive cyclone over the Sea of Japan. Nuss and Kamikawa (1990) report that the ageostrophic circulation associated with a downstream upper-level jet streak (e.g., Uccellini et al. 1987) maintains strong surface fluxes, which are attributed to the maintenance of the warm front gradient in the ascending region, leading to an explosive cyclogenesis over the northwestern Pacific Ocean.

These studies clarified the existence of a sensitive mechanism—or a combination of mechanisms—for explosive cyclogenesis in specific cases. To the authors' knowledge, Yoshida and Asuma (2004) and Kuwano-Yoshida and Asuma (2008) conduct the first statistical studies on the mechanisms underlying the development

Corresponding author address: Akira Kuwano-Yoshida, Earth Simulator Center, Japan Agency for Marine-Earth Science and Technology, 3173-25, Showa-machi, Kanazawa-ku, Yokohama, Kanagawa, 236-0001, Japan.
E-mail: akiray@jamstec.go.jp

DOI: 10.1175/MWR-D-12-00161.1

of explosive cyclones. Yoshida and Asuma (2004) categorize explosive cyclones developing in the northwestern Pacific region into two types according to whether the region of the most rapid development is in the Sea of Okhotsk or Sea of Japan (OJ) or in the northwestern Pacific Ocean (PO). These authors conduct a cyclone-relative composite analysis to investigate the relationships between development mechanisms and environments for the two types of explosive cyclones. They suggest that the cyclone-relative structures of the upper jet streak, near-surface temperature front, and moisture fields during explosive cyclone development differ significantly between OJ and PO explosive cyclones in response to seasonal variations in climatological jet strength, baroclinic zone, and moisture distribution. Yoshida and Asuma (2004) further suggest that the large-scale climatological environment, which depends on land–sea distribution and seasonal cycles, controls the relative contribution of each physical mechanism to explosive cyclogenesis over the northwestern Pacific region. Kuwano-Yoshida and Asuma (2008) demonstrate that typical PO explosive cyclones rarely develop without the latent heat release associated with condensation—whereas OJ explosive cyclones may develop without such latent heat release—by conducting sensitivity examinations using the fifth-generation Pennsylvania State University–National Center for Atmospheric Research (PSU–NCAR) Mesoscale Model (MM5). These results suggest that large-scale environmental analysis may help to understand differences in sensitive development mechanisms and to improve prediction accuracy for individual explosive cyclones.

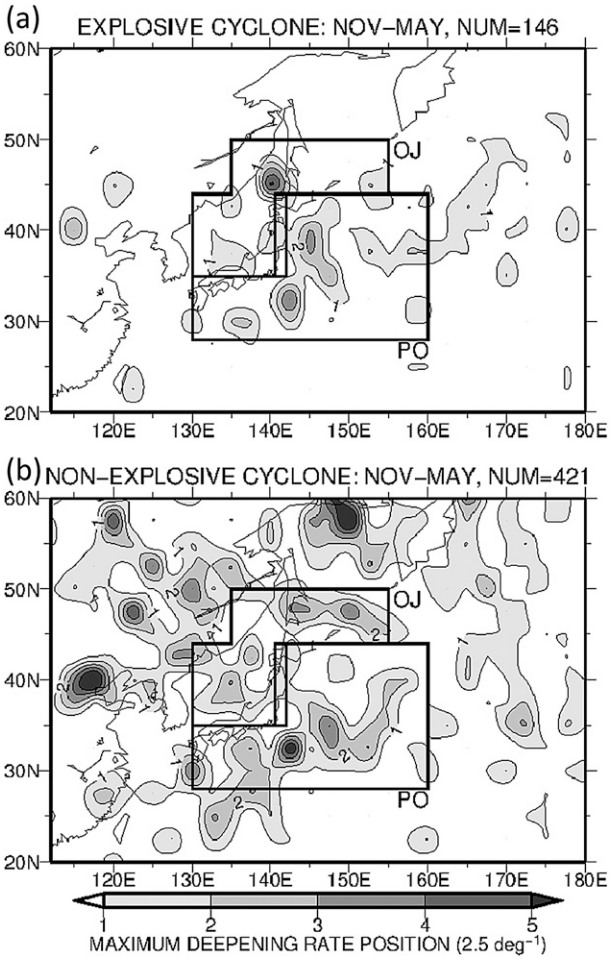

FIG. 1. Density map of the maximum deepening rate position for (a) explosive cyclones and (b) nonexplosive cyclones. The areas framed by bold lines are the OJ and PO cyclone areas.

Although it can be difficult to predict explosive cyclones accurately, continuous efforts in developing and improving numerical weather prediction models, data assimilation methods, and observation systems have led to an improvement in overall forecasting capabilities (Shapiro et al. 2010). Forecasting experiments investigating the sensitivity of numerical models to parameterization and reliability evaluations of operational weather prediction systems have also been conducted, specifically for extratropical cyclones. Kuo and Low-Nam (1990) suggest that the crucial components for the short-range (0-24 h) prediction of rapid deepening within a regional model include the initial conditions, the horizontal grid resolution, the precipitation parameterization, and lateral boundary conditions. The first three components may also apply to global models. Harr et al. (1992) examine the 72-h forecast errors of North Pacific maritime cyclones using the Navy Operational Global Atmospheric Prediction System (NOGAPS) and report that NOGAPS tends to overestimate cyclone deepening more to the left of track over the western Pacific and underestimate it more to the right of track over the central Pacific. Both track and deepening rate errors occur at similar positions, and these authors hypothesize that the difference may be caused by the relative importance of adiabatic and diabatic processes in each region. Ensemble forecasting is one way to investigate the influence of initial conditions because in ensemble forecasting multiple forecasts are started from slightly different initial conditions at one time. Sanders et al. (2000) analyze ensemble forecasts with 31 members at ranges of 2–5 days for two explosive cyclones. They suggest that the central sea level pressure (SLP) of the explosive cyclone associated with the strong preceding trough at 500 hPa has better predictability, whereas that of the other explosive cyclone associated with the weak trough is less predictable. A series of studies by Froude (Froude et al. 2007a,b; Froude 2009, 2010, 2011) report that forecast errors of extratropical

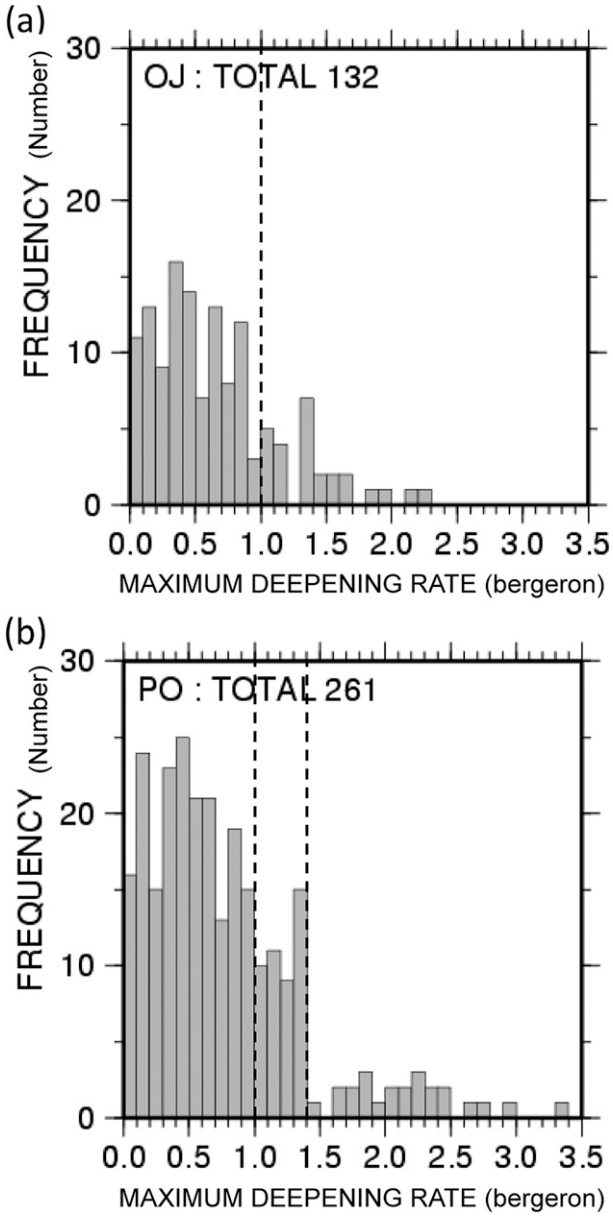

FIG. 2. Frequency distribution of the maximum deepening rate (number) for (a) Okhotsk-Japan Sea (OJ)-type and (b) Pacific Ocean (PO)-type cyclones. Dashed lines correspond to measurements of 1.0 and 1.4 Bergeron.

cyclones differ by the operational ensemble prediction system and that propagation speed is slower than the analysis for all systems. However, the reasons for these error differences among the systems and locations of cyclones are not understood.

In recent years, ensemble Kalman filter (EnKF) methods for data assimilation have become popular because the data assimilation can be readily performed in ensemble forecast systems using massively parallel computers. The Canadian Meteorological Centre applies an EnKF method to the operational ensemble prediction system (Houtekamer et al. 2005). Miyoshi et al. (2007) produced experimental reanalysis data by using a local ensemble transform Kalman filter (LETKF) data assimilation system (Miyoshi and Yamane 2007). An advantage of ensemble-based assimilation systems is the ability to estimate spatial analysis error distribution and its evolution over time based on the spread of the ensemble members. Using mesoscale ensemble forecast datasets Zhang (2005) shows that maximum error growth in a winter cyclone occurred in the vicinity of the strongest potential vorticity gradient over the area of active moist convection at the upper level and surface, and the ensemble spreads depend on the complicated flow pattern in a winter cyclone. However, the general structures of prediction error within extratropical cyclones have not been reported.

TABLE 1. The occurrence number of cyclones by category.

OJ B	OJ C	PO A	PO B	PO C
24	24	23	39	50

In this paper, we present our investigation of forecast errors and initial condition uncertainties for explosive cyclogenesis in the northwestern Pacific region using an ensemble reanalysis. The distribution of the cyclone-relative prediction error for both the increment and the ensemble spread are statistically analyzed, and the relationship between error distribution and explosive cyclogenesis mechanisms influenced by large-scale environmental conditions are investigated. A description of the data and analysis methods are presented in section 2. Cyclone-relative composite analyses for the increments and the ensemble spreads are presented in section 3. Finally, a summary and conclusions are presented in section 4.

2. Data and methods

In this study, we use the AGCM for the Earth Simulator (AFES; Ohfuchi et al. 2004; Enomoto et al. 2008) LETKF Experimental Re-Analysis (ALERA; Miyoshi et al. 2007). ALERA is generated by a data assimilation system comprising AFES with T159L48 resolutions and LETKF (Miyoshi and Yamane 2007). Observations used in numerical weather prediction by the Japan Meteorological Agency operations are assimilated, with the exception of satellite radiances. ALERA was produced from 1 May 2005 to 10 January 2007. The horizontal resolution of the product is 1.25° with 17 vertical levels from 1000 to 10 hPa. ALERA outputs SLP,

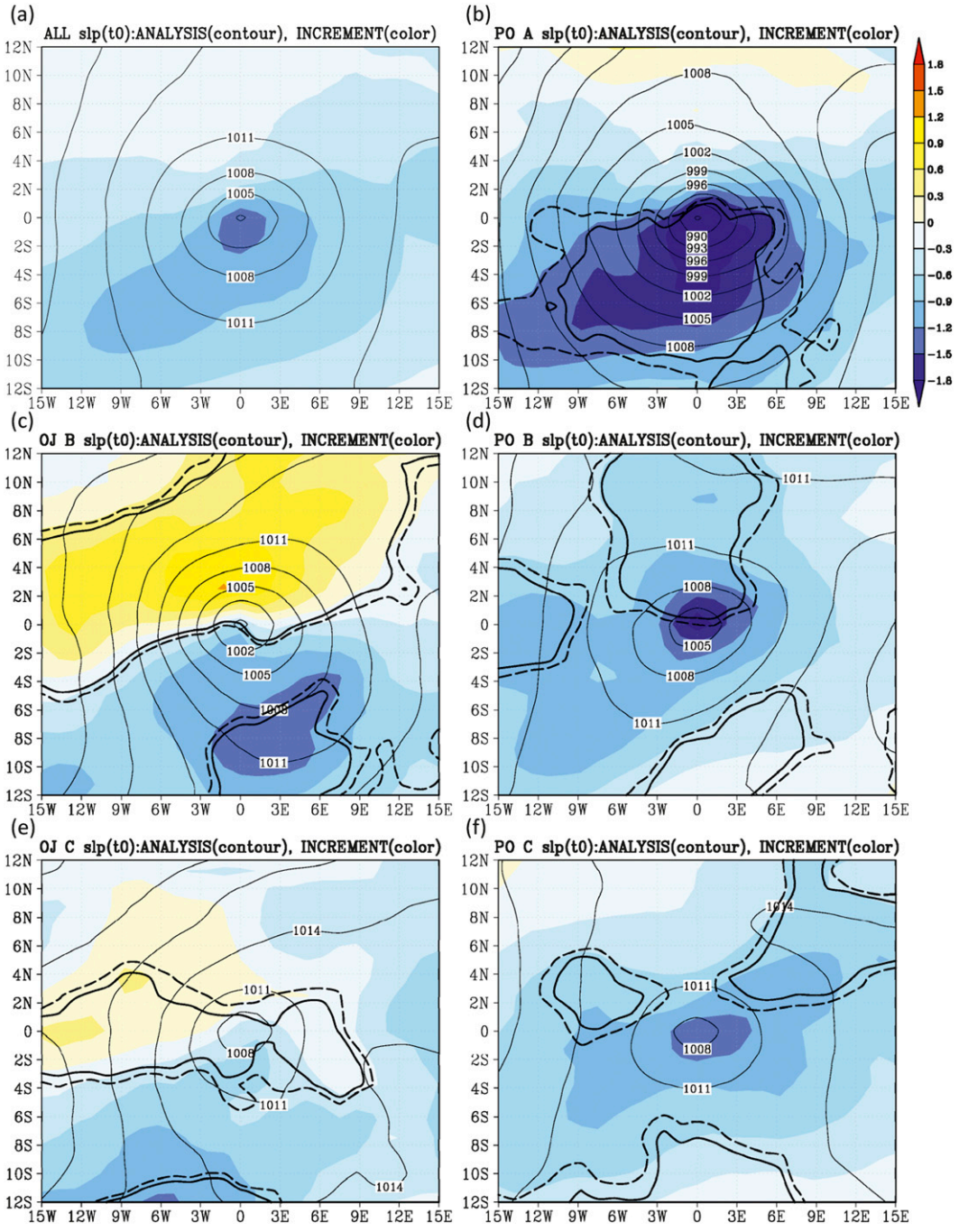

FIG. 3. Cyclone-relative composites of sea level pressure increments (shaded, hPa) and sea level pressure (thin contour lines, hPa) at the end of the 6-h period of the maximum deepening rate for (a) all categories, (b) PO A, (c) OJ B, (d) PO B, (e) OJ C, and (f) PO C cyclones. The bold solid line and the bold dashed line show the 95% and 90% significance level, respectively, of the *t* tests for the average of all other cyclone categories. Axes are the longitude and latitude relative to the cyclone center.

geopotential height, horizontal winds, temperature, and dewpoint depression. The 6-h ensemble mean and spread of the analysis and the first guess of these variables produced from 40 members are available 4 times per day. All 40 ensemble members of the analysis and the first guess are available daily. The spread is defined as the standard deviation among the 40 members. The first guess is the 6-h forecast from the analysis. The

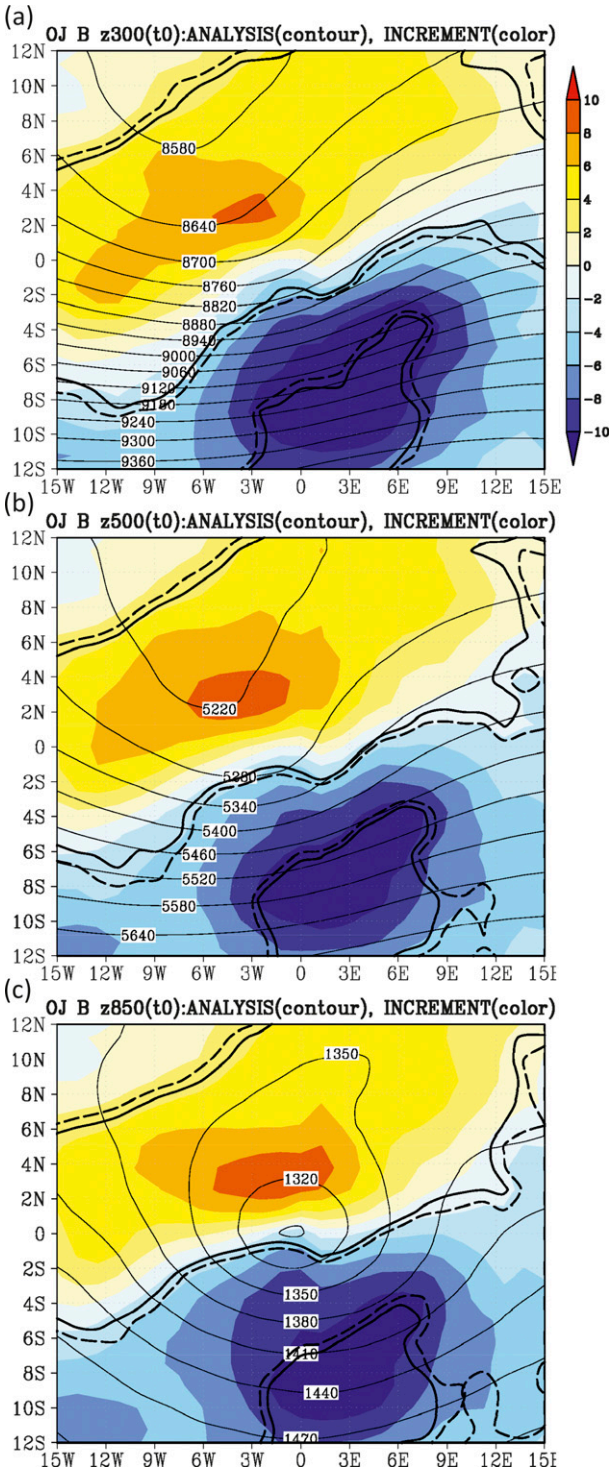

FIG. 4. Cyclone-relative composites of geopotential height increments (shaded, m) and geopotential height (contour lines, m) at (a) 300, (b) 500, and (c) 850 hPa for OJ B cyclones at the time of the maximum deepening rate. The bold solid line and the bold dashed line show the 95% and 90% significance level, respectively, of *t* tests for the average of all other cyclone categories.

analysis increment is defined as the difference between the analysis mean and the first-guess mean. In this study, the increment is used as a measure of 6-h forecast error. Although the increment includes error information from the model, analysis method, and observation, the increment in the analyzed area (Fig. 1) shows similar distribution to that normalized by the annual standard deviation in time at a given grid point, suggesting lower impact of systematic error from observation density on the increment. To investigate a 6-h cyclogenesis, we reproduce the 6-h analysis of each ensemble member from that of the daily analysis by linear interpolation in time. The ensemble mean of the 6-h interpolated analyses is equal to the original 6-h analysis mean. Both spreads of analyses and first guesses are normalized by the annual standard deviation in time between 0000 UTC 1 June 2005 and 1800 UTC 31 May 2006 at a given grid point to remove the influence of background spread associated with observation density. This normalization procedure is conducted because the ensemble spread is small over land—especially in Europe, North America, and East Asia, where there are dense observations—whereas the spread is large over the ocean, in general (e.g., Fig. 8 in Moteki et al. 2011). The normalized spreads of analysis and first guess can be used as indices of model and initial condition uncertainties depending on flow. Grid points with large normalized first-guess spreads indicate that the forecast at such points is sensitive to the initial condition. Grid points with large normalized analysis spreads indicate that the analysis has a large flow-dependent uncertainty at such points. These analyses are applied to developing cyclones to understand the uncertainty distribution.

A cyclone is defined as an SLP horizontal minimum in the 6-h analysis mean data. Cyclones are tracked using the nearest-neighbor method (e.g., Blender and Schubert 2000), in which a detected cyclone is linked to the nearest detected cyclone occurring within 6 h and 800 km. The cyclone deepening rate (CDR, in units of Bergeron), which is analogous to the 12-h cyclone deepening rate in Yoshida and Asuma (2004), is defined as follows:

$$\mathrm{CDR} = \left[\frac{p(t-6)-p(t)}{6}\right]\left[\frac{\sin 60^\circ}{\sin\dfrac{\phi(t-6)+\phi(t)}{2}}\right], \quad (1)$$

where t is the analyzed time (in hours), p is the central SLP (in hPa), and ϕ is the central latitude (in degrees). Note that the deepening rate is estimated by the 6-h central pressure change to determine predictability in a 6-h forecast instead of changes over 24 h (Sanders and Gyakum 1980) or 12 h (Yoshida and Asuma 2004), as in the case of previous works. Although the 6-h calculation

of SLP change may be affected by mesoscale phenomena like inertia–gravity wave (Koppel et al. 2000), the influence is probably small in this study, because the central pressure change analysis is based on Lagrangian synoptic cyclone tracking. Cyclones whose deepening rates are equal to or greater than 1 Bergeron are defined as explosive cyclones; other cyclones are defined as nonexplosive cyclones. Cyclones that occur in cold seasons from November to May in the sector between 20°–60°N and 100°E–180° are detected.

Figure 1 shows the frequency–density maps of maximum deepening rate positions for each explosive and nonexplosive cyclone in the cold season from November to May. Most explosive cyclones develop rapidly over water between 30° and 50°N (Fig. 1a), whereas nonexplosive cyclones may develop over both land and water (Fig. 1b). The explosive cyclone distribution resembles the long-term analysis in Chen et al. (1992), although only two cold seasons are analyzed in the present study. Following Yoshida and Asuma (2004), cyclones are divided into two categories: OJ cyclones and PO cyclones. The analysis areas of OJ and PO cyclones are based on the explosive cyclone frequency between 28°–50°N and 130°–160°E, as shown in Fig. 1, because most explosive cyclones develop there. The cyclones studied include 132 OJ cyclones and 261 PO cyclones.

Figure 2 shows histograms of the maximum deepening rates in the cyclone lifetime for OJ and PO cyclones. The maximum deepening rates of the OJ cyclones reach a maximum of 2.3 Bergeron, and two main peaks are evident on either side of the 1.4-Bergeron interval. By contrast, the PO cyclones are characterized by a long-tailed distribution pattern in their maximum deepening rates from 1.4 up to 3.4 Bergeron. The long-tailed distribution of greater deepening rates in PO cyclones is caused by an amplification of cyclogenesis by the diabatic mechanism in PO explosive cyclones (Yoshida and Asuma 2004; Kuwano-Yoshida and Asuma 2008; Roebber and Schumann 2011). Because OJ explosive cyclones usually develop through a dry mechanism (Yoshida and Asuma 2004; Kuwano-Yoshida and Asuma 2008), the frequency of large maximum deepening rates is smaller than that for PO cyclones. Indeed, the difference in the maximum deepening rate distribution is consistent with the results of Yoshida and Asuma (2004), although they analyze only explosive cyclones defined by a 12-h deepening rate.

To determine the dependency of cyclone predictability on the maximum deepening rate, PO explosive cyclones are categorized as category A (CDR $\geq$ 1.4 Bergeron) and category B (1.0 $\leq$ CDR $<$ 1.4 Bergeron). In addition, category C (0.5 $\leq$ CDR $<$ 1.0 Bergeron) are analyzed. Note that category B of OJ cyclones include category A to maintain a statistically large enough number in the sample. As a result, cyclones are analyzed by five categories; OJ B, OJ C, PO A, PO B, and PO C cyclones. The sampling number for each category is summarized in Table 1.

To examine the physical mechanisms underlying cyclone deepening, the extended Zwack–Okossi development equation (Z-O equation; Zwack and Okossi 1986; Lupo et al. 1992) is used. This equation describes the geostrophic relative vorticity tendency at the lower boundary as a result of dynamic and thermodynamic forcing vertically integrated in the atmosphere. This equation has an advantage over the Petterssen–Sutcliffe development equation because the Z-O equation can be integrated up to a given vertical level and does not require a level at which the vertical velocity is zero. This advantage enables the easy application of the Z-O equation for synoptic-scale cyclone and anticyclone analyses with typical grid data. For example, Tilly et al. (2008) use the Z-O equation to diagnose blocking and cyclone mechanisms in the Southern Hemisphere. In the present study, 925 hPa is chosen as the lower boundary level—which is the second lowest level in ALERA—because central cyclone SLP is often lower than 1000 hPa, whereas 850 hPa (the next level) is too high to capture near-surface processes. The equation can be written as follows:

$$\frac{\partial \zeta_{gp_b}}{\partial t} = \frac{1}{p_b - p_t}\int_{p_t}^{p_b}(-\mathbf{V}\cdot\nabla\zeta_a)\,dp - \frac{1}{p_b - p_t}\int_{p_t}^{p_b}\left[\frac{R}{f}\int_{p}^{p_b}\frac{\nabla^2(-\mathbf{V}\cdot\nabla T)}{p}dp\right]dp$$
$$-\frac{1}{p_b - p_t}\int_{p_t}^{p_b}\left[\frac{R}{f}\int_{p}^{p_b}\frac{\nabla^2(\dot{Q}/c_p)}{p}dp\right]dp - \frac{1}{p_b - p_t}\int_{p_t}^{p_b}\left\{\frac{R}{f}\int_{p}^{p_b}\frac{\nabla^2[-(T/\theta)(\partial\theta/\partial p)\omega]}{p}dp\right\}dp$$
$$= \mathrm{VADV} + \mathrm{TADV} + \mathrm{LATH} + \mathrm{ADIA}, \qquad (2)$$

where p is the pressure; p_b is the lower boundary layer pressure of 925 hPa; p_t is the upper boundary pressure, which is 50 hPa in the present study; $\mathbf{V}$ is the horizontal wind velocity; ∇ is the horizontal gradient operator, ζ_{gp_b}

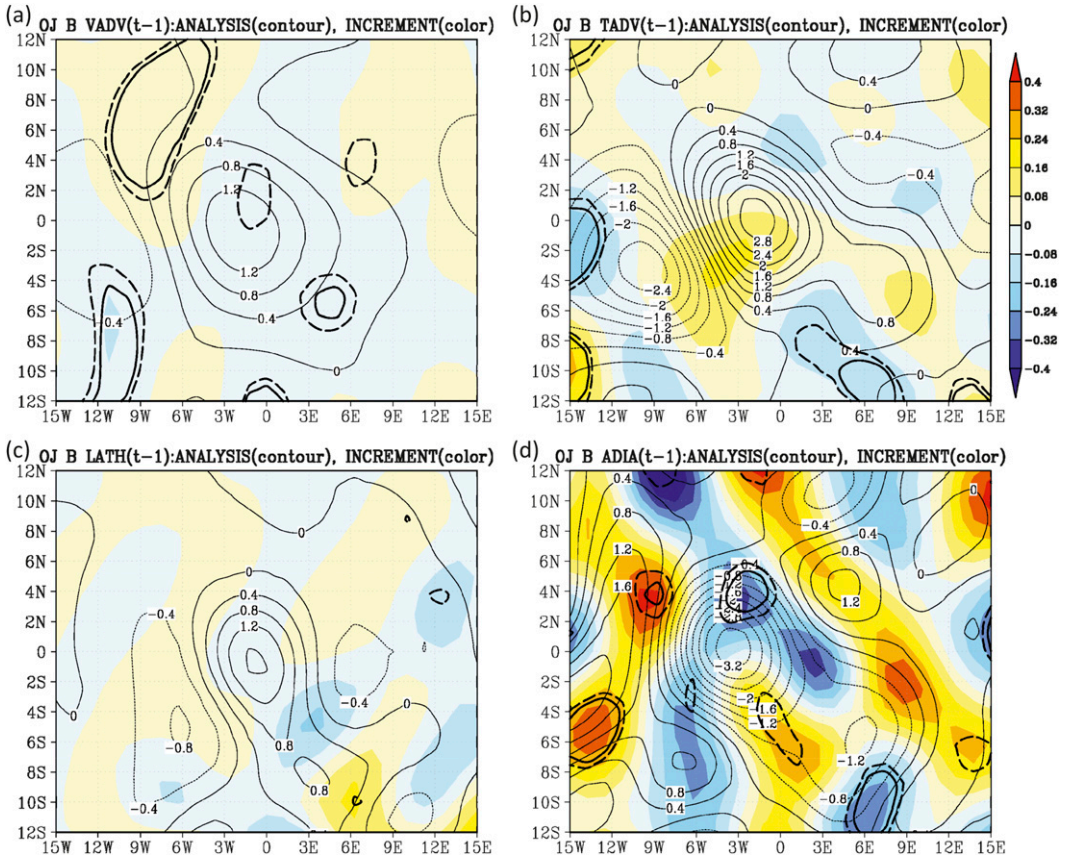

FIG. 5. OJ B cyclone-relative composites of Z-O equation terms' increments (shaded, $10^{-9}\,s^{-2}$) and their analyses (contour lines, $10^{-9}\,s^{-2}$) at 6 h prior to the time of the maximum deepening rate, including (a) VADV, (b) TADV, (c) LATH, and (d) ADIA. The bold solid line and the bold dashed line show the 95% and 90% significance level, respectively, of the *t* test for the average of all other cyclone categories, respectively.

is the geostrophic relative vorticity in the lower boundary layer; ζ_a is the absolute vorticity; f is the Coriolis parameter; R is the gas constant of dry air; $\dot{Q}$ is the diabatic heating and cooling rate; c_p is the specific heat at constant pressure; T is the temperature; θ is the potential temperature; and ω is the vertical motion in isobaric coordinates. VADV represents the effect of horizontal advection of the absolute vorticity, TADV represents the effect of local extrema of horizontal temperature advection, LATH represents the effect of localized diabatic heating, and ADIA represents the effect of localized adiabatic warming associated with vertical motion. The vertical velocities are calculated by the kinematic method (O'Brien 1970). The diabatic heating rate is calculated according to Yoshida and Asuma (2004), in which the grid-scale latent heat is calculated based on the upward motion, relative humidity, and vertical gradient of specific humidity (Krishnamurti and Moxim 1971; Vincent et al. 1977), and the convective latent heat release is calculated by Kuo's parameterization scheme (Kuo 1965, 1974), as improved by Edmon and Vincent (1976), Lin and Smith (1979), and Smith et al. (1984). Although the surface sensible and latent heat fluxes over the Kuroshio may affect cyclone developments as shown by Nuss and Kamikawa (1990), these terms are neglected in the present study because they are implicitly included in TADV and LATH through the temperature and moisture fields. Each value is smoothed by the two-dimensional second-order filtering scheme developed by Shapiro (1970) to reduce subsynoptic-scale noise of less than 800-km wavelength and calculated for all members of the 6-h analyses to estimate the analysis spread. The filter is more sophisticated than the simple five-point average used in Lupo et al. (1992), which depends on grid space. The result is not as sensitive to filtering methods if the subsynoptic-scale noise is filtered out adequately. Each term in Eq. (2) calculated from the ensemble means of the analysis and the first guess is used to estimate the increment.

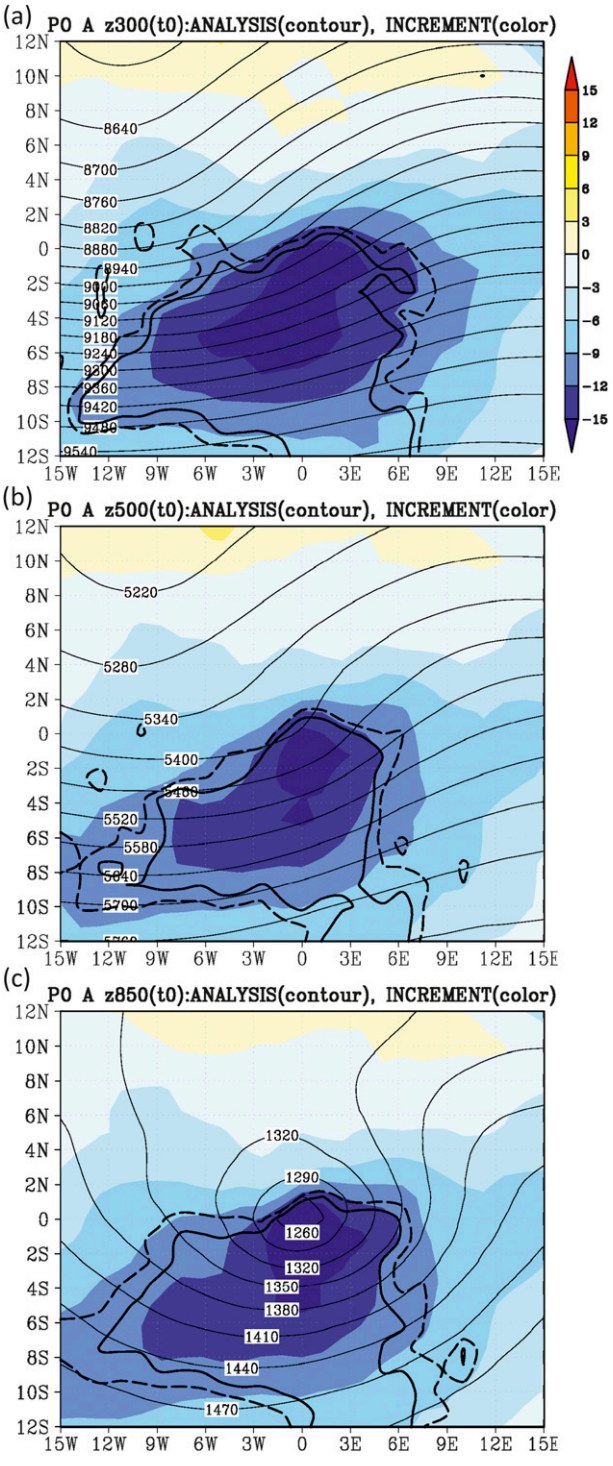

FIG. 6. As in Fig. 4, but for PO A cyclones.

To determine the prediction error structure and its relationship to the OJ and PO cyclone structures at the time of the maximum deepening rate, the cyclone-relative composite analysis is performed in a manner similar to that of Yoshida and Asuma (2004). Cyclone centers at the time of the maximum deepening rate [t = t0 at the end of the 6-h deepening period in Eq. (1)] are overlapped, and variables are averaged for each category. The statistical significance of the composite for each cyclone category is estimated by t test against the mean of the composite at the same time for the all other cyclone categories to determine whether the composite structure is characteristic of the category.

3. Results

a. *Increment analysis*

Figure 3 shows composites of the SLP analysis mean and its increment at t = t0 for each category. The blue shade indicates that the analysis SLP is lower than the first-guess SLP: the model underestimates cyclone intensity compared to the analysis. Yellow and red shades indicate that the model overestimates cyclone intensity. SLP increments for OJ B cyclones show a meridional dipole pattern (Fig. 3c). The first-guess estimates a lower SLP in the northern part of the cyclone and a higher SLP in southern part than does the analyzed SLP. Thus, the forecast cyclone is too far north compared to the analyzed cyclone position. Similar characteristics can be observed in OJ C cyclones (Fig. 3e), but the magnitudes and areas of positive increment with high significance are weaker and shift more to the west than that of OJ B cyclones. By contrast, PO cyclones show negative increments over the cyclone centers: the forecast PO cyclones are too weak (Figs. 3b,d,f). The negative increment magnitude increases together with the deepening rate. Among PO cyclones, PO A cyclones show the largest negative increments or the largest forecast errors.

Figure 4 shows composites of the analysis means and increments of the geopotential height of OJ B cyclones. The horizontal distribution of increments at 850 hPa (Fig. 4c) is similar to that of SLP increments (Fig. 3c), whereas positive increments over the northern side tilt to the west with increasing height (Figs. 4a,b). Because the center of the positive increments corresponds to the southern edge of the upper trough (Fig. 4a) and because the westward-tilting trough contributes to OJ B cyclone development (Yoshida and Asuma 2004), it is believed that the increment is related to the upper trough prediction error of the first guess. Thus, these findings suggest that the upper-level trough does not extend far enough south in the forecast and that the forecast surface cyclone is located north of the analyzed cyclone. The increment feature seems to contradict the results of Froude (2010), who shows that propagation speed is

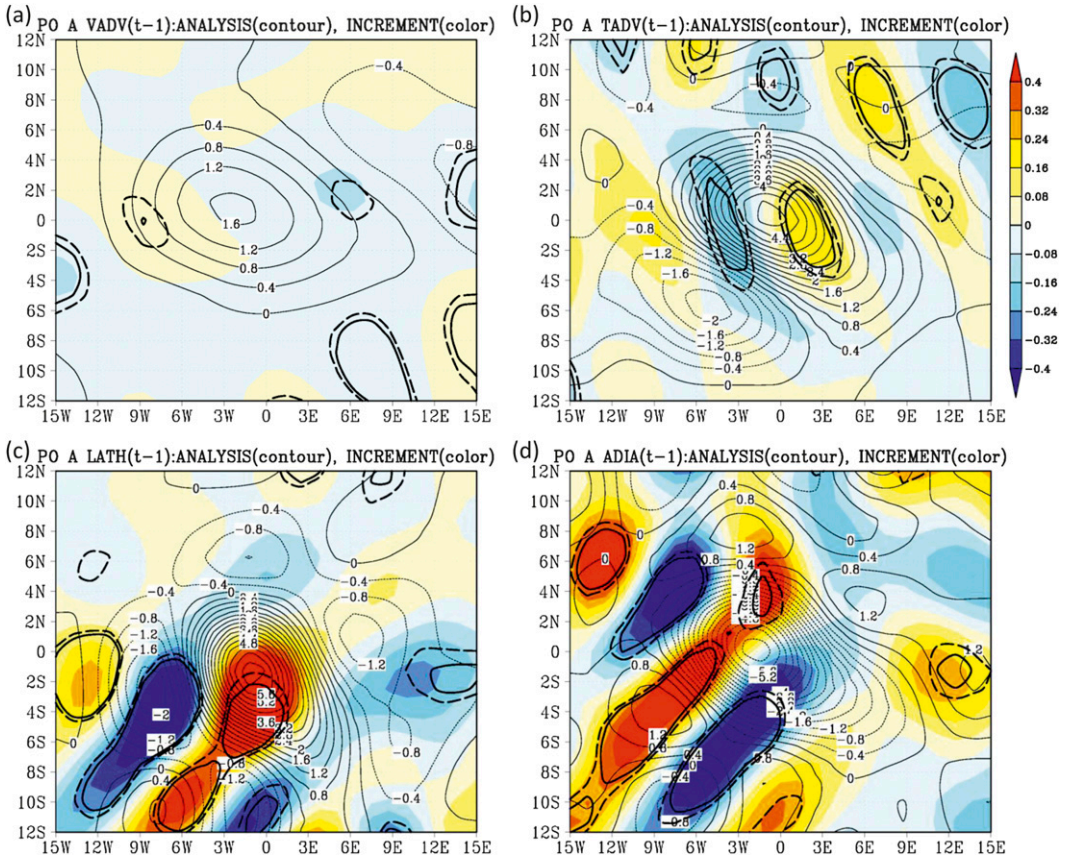

FIG. 7. As in Fig. 5, but for PO A cyclones.

slower than the analysis for all systems in the The Observing System Research and Predictability Experiment (THORPEX) Interactive Grand Global Ensemble (TIGGE). However, Froude's paper treats all extratropical cyclones in the Northern Hemisphere without classifying them by strength, deepening rate, or developing region. Therefore, there is a need to conduct similar analysis in the present study using TIGGE in the future.

Figure 5 shows composites of four terms on the right-hand side of the Z-O equation—VADV, TADV, LATH, and ADIA—in addition to their increments for OJ B cyclones. To compare these terms with the SLP increment (taken as the prediction error of the local SLP tendency from 6 h earlier), the terms estimated at t0 − 6 h are composited for cyclone centers at t0. Note that the sign of the increment of 925-hPa vorticity tendency is the opposite of that of the SLP: a positive vorticity tendency would be expected to correspond to a negative SLP tendency, and vice versa. VADV shows a negative increment north of the cyclone center and a highly significant positive increment to the northwest (Fig. 5a), which indicates that the first guess overestimates positive vorticity advection to the north of the cyclone. This finding is consistent with the geopotential height error associated with the upper trough (Fig. 4a) because VADV is large at the upper levels (Yoshida and Asuma 2004); however, the magnitude of the VADV increment is the smallest among the four terms. Although the TADV contributes the most to the development of local vorticity over the cyclone, there is no significant increment (Fig. 5b). LATH also shows a weak significance with a weak contribution to cyclone development (Fig. 5c), which is similar to the results reported by Yoshida and Asuma (2004). ADIA works to decrease vorticity over the cyclone center—in contrast to the other terms (Fig. 5d)—because the cyclone center is covered by the updraft. Highly significant negative increments appear to the northwest of the cyclone center, similar to VADV. The large increment of ADIA over the northwestern area of the cyclone indicates that the first guess predicts earlier eastward propagation of the upper trough associated with tropopause folding because ADIA is a product of vertical velocity and static stability and because tropopause folding causes the vertical intrusion of large static stability from the stratosphere. These results suggest that forecast errors associated with upper trough

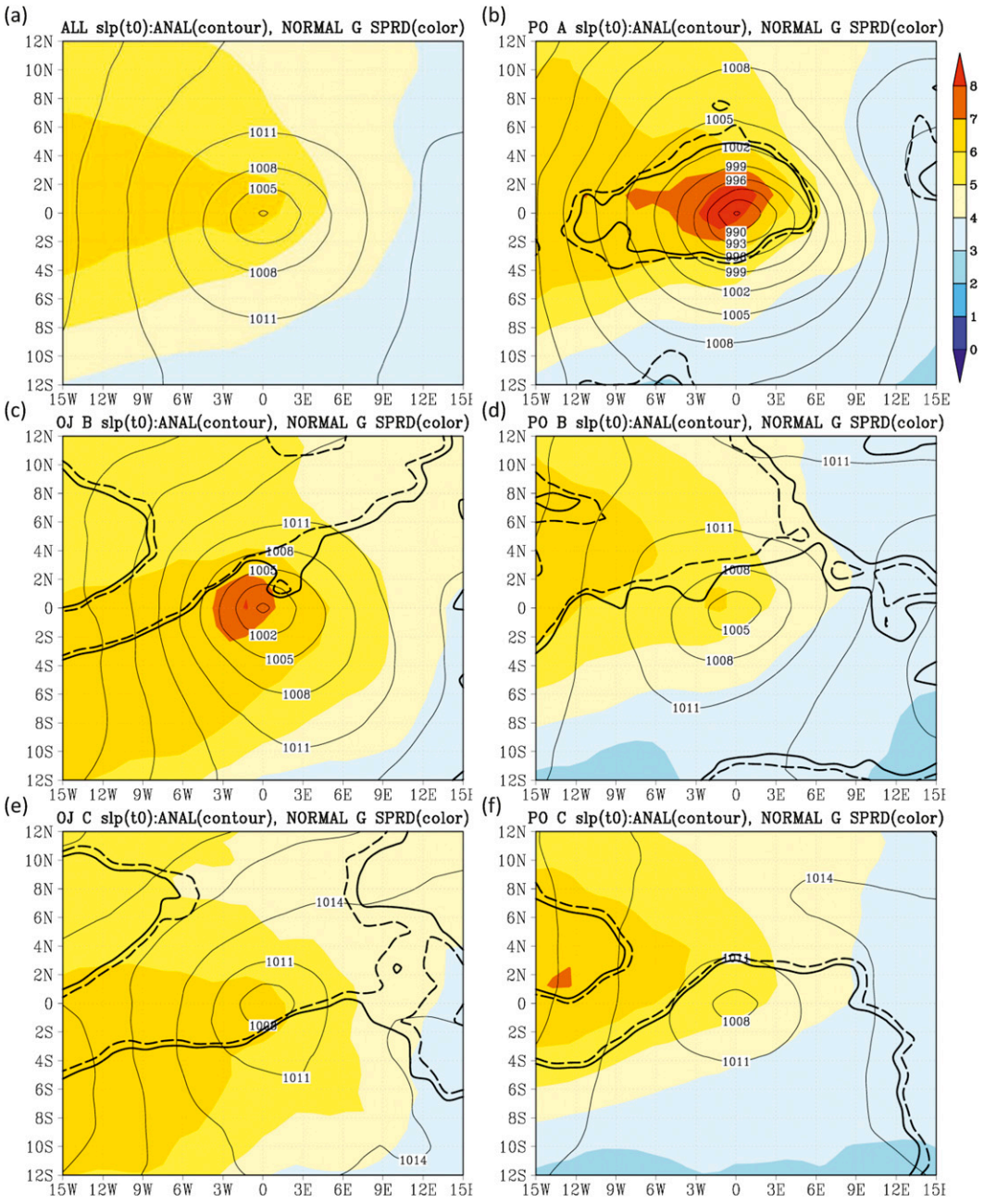

FIG. 8. Cyclone-relative composites of SLP-normalized first-guess spreads (color) and analyses (contour lines, hPa) at the time of maximum deepening rate for (a) all categories, (b) PO A, (c) OJ B, (d) PO B, (e) OJ C, and (f) PO C cyclones. The bold solid line and the bold dashed line show the 95% and 90% significance level, respectively, of *t* tests for the average of all other cyclone categories.

position error are related to surface cyclone position errors in OJ B cyclones in AFES, whereas latent heat release and temperature advection errors are not significant.

With respect to PO A cyclones, a large, highly significant negative increment of geopotential height is observed around the cyclone center and near the southern side, whereas the upper trough and the associated increment are weaker than those of OJ B cyclones (Fig. 6a). In general, this increment distribution signature can be observed from the surface (Fig. 6c) to 300 hPa (Fig. 6a). These results suggest that both the upper troughs and surface cyclone forecasts are too weak for PO A cyclones.

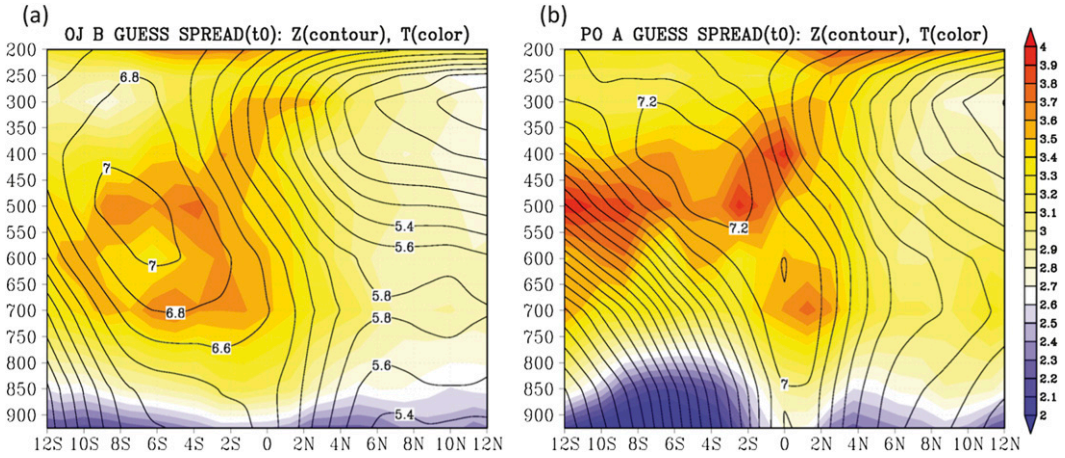

FIG. 9. Meridional vertical cross section of cyclone-relative composites of first-guess spreads of geopotential heights (contour lines, m) and temperature (color, K) at the time of the maximum deepening rate for (a) OJ B and (b) PO A cyclones, which are zonally averaged from the cyclone center longitude to 15° westward.

The increment distributions of the Z-O equation of PO A cyclones are also different from those of OJ B cyclones. The VADV increment is small, with no significance near the cyclone center (Fig. 7a). The TADV increment in Fig. 7b is positive to the east of the center of the cyclone and negative to the west of the center of the cyclone, and its magnitude is smaller than that of LATH. The LATH contribution to the vorticity tendency is much larger than that of the OJ B cyclones (Fig. 7c). Its positive increment is also large, with high significance to the south of the cyclone center, whereas its negative increment appears southwest of cyclone. ADIA also shows a large increment wave pattern to the west of the cyclone, whereas the increment sign of ADIA tends to be opposite to that of LATH (Fig. 7d). Considering that both ADIA and LATH are influenced by vertical motion, the overlap of their increments suggests that the vertical motion error associated with cloud condensation is significant for the prediction of PO A cyclones. This result reveals that the LATH positive increment is a primary contributor to the negative SLP increment around the cyclone center, although part of it is absorbed by ADIA increment. The composite analysis of increments for OJ and PO explosive cyclones suggests that errors associated with the important mechanisms involved in explosive cyclone development are amplified and affect the prediction of the development of explosive cyclones, and the increments of weak cyclogenesis are weaker than explosive cyclogenesis.

b. Spread analysis

As discussed in section 2, an analysis of the ensemble first-guess spread, which is not provided by existing reanalysis data, is useful in understanding the uncertainty of the initial conditions associated with rapid deepening. Figure 8 shows the normalized first-guess spread of SLP at the time of the maximum deepening rate for the five cyclone categories. OJ B and C cyclones have a large spread just west of the cyclone center that elongates to the southwest (Figs. 8c,e), whereas the increment shows a meridional dipole distribution (Figs. 3c,e). OJ B cyclones show a maximum spread just to the northwest of the cyclone center (Fig. 8c). Conversely, PO A, B, and C cyclones show a large spread from the cyclone center to the northwest (Figs. 8b,d,f). PO A cyclones show a large spread around the cyclone center, in particular (Fig. 8b): weaker cyclones show a large spread far from the cyclone center (Figs. 8d,f).

Figure 9 shows the meridional vertical cross sections of the geopotential height and temperature spreads zonally averaged between the cyclone center and 15°W of the cyclone center. The region with the largest spread of the geopotential height almost overlaps the largest temperature spread for both OJ B and PO A cyclones (Figs. 9a,b). However, the vertical structures of OJ B and PO A cyclones are different. For OJ B cyclones, a large spread area tilts to the south with height, at a maximum of 750–400 hPa (Fig. 9a). For PO A cyclones, a large spread area extends vertically over the cyclone center and tilts to the south from 500 hPa (Fig. 9b). It is notable that the temperature spread shows a minimum at the lowest level, whereas the geopotential height spread shows a maximum at the cyclone center at the level. The small spread of near-surface temperature is a result of the fact that a single sea surface temperature (SST) field is used as a boundary condition to each

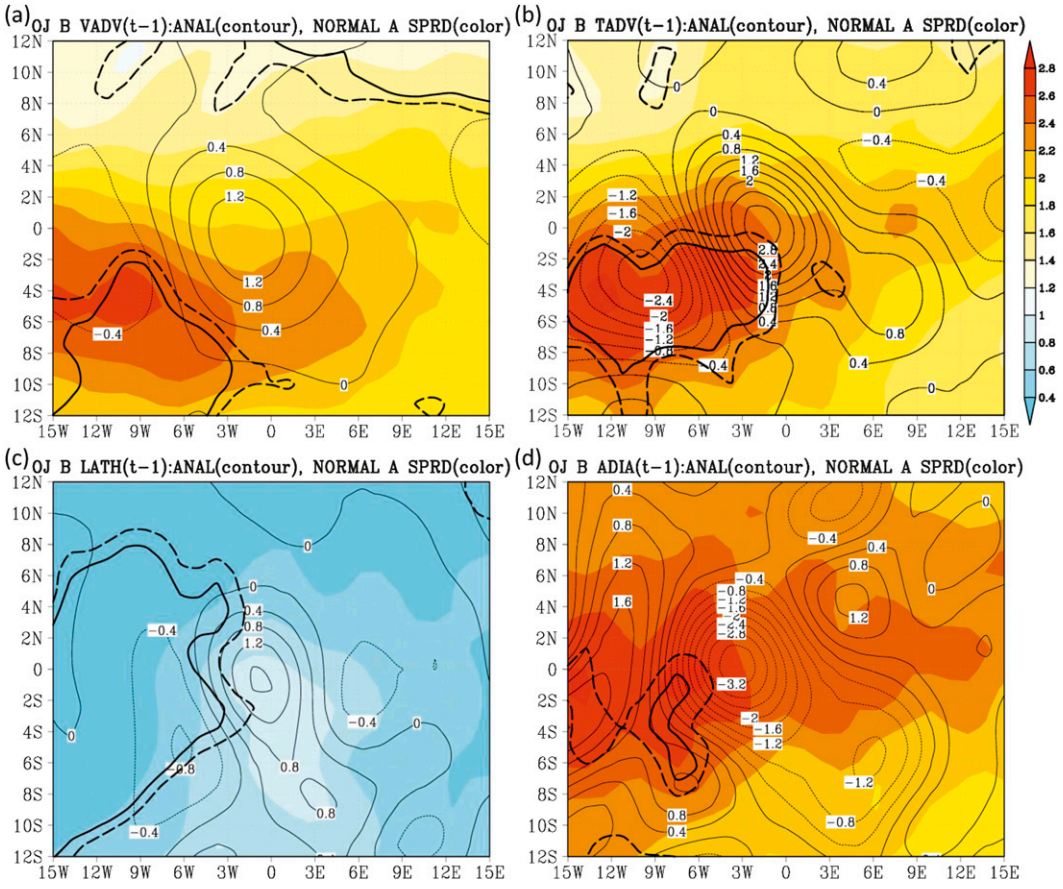

FIG. 10. OJ B cyclone-relative composites of the analysis spreads of Z-O equation terms normalized by the local standard deviation of each term for time (shaded, no unit) and their analysis (contour lines, $10^{-9}\,s^{-2}$) at 6 h prior to the time of the maximum deepening rate, including (a) VADV, (b) TADV, (c) LATH, and (d) ADIA. The bold solid line and the bold dashed line show the 95% and 90% significance level, respectively, of the *t* test for the average of all other cyclone categories.

ensemble member. Kunii and Miyoshi (2012) report that the uncertainties of SST increase the spread near the surface in LETKF with a regional model. Because the geopotential height depends mainly on the air mass above the level, the spread near the surface is mainly influenced by atmospheric disturbances rather than SST.

These structures can primarily be explained by the Z-O equation value spreads. For OJ B cyclones, the TADV, VADV, and ADIA spreads are large over the southwestern side of the cyclone with high significance (Figs. 10a,b,d)—which is consistent with the SLP and geopotential height spread distributions (Figs. 8 and 9)—whereas the LATH spread is small (Fig. 10c). The peaks of the VADV, TADV, and ADIA spreads are located on the southwestern side of the positive analysis peaks. This distribution is consistent with Zhang (2005), who reports that larger spreads are located near large potential vorticity (PV) gradients. These results suggest that wind and temperature observations around the southwestern quadrant of the cyclone may alleviate the uncertainty in the predictability of OJ B cyclones. In fact, dropsondes have been released in this area during the target observation component of the winter THORPEX Pacific Asian Regional Campaign (T-PARC; Majumdar et al. 2010). However, it is difficult to directly compare the spread distribution with the SLP spread because the Z-O composite uses spread normalized by its own standard deviation, for a time at a particular grid. Thus, another normalized spread is introduced, which is normalized by the standard deviation of the sum of the VADV, TADV, LATH, and ADIA. The alternative normalized spread represents the relative contribution to the total vorticity tendency spread (Fig. 11). VADV and LATH spreads show only a small contribution, although they show high significance over the southwestern and western region, respectively (Figs. 11a,c). The ADIA spread shows a large contribution over the west

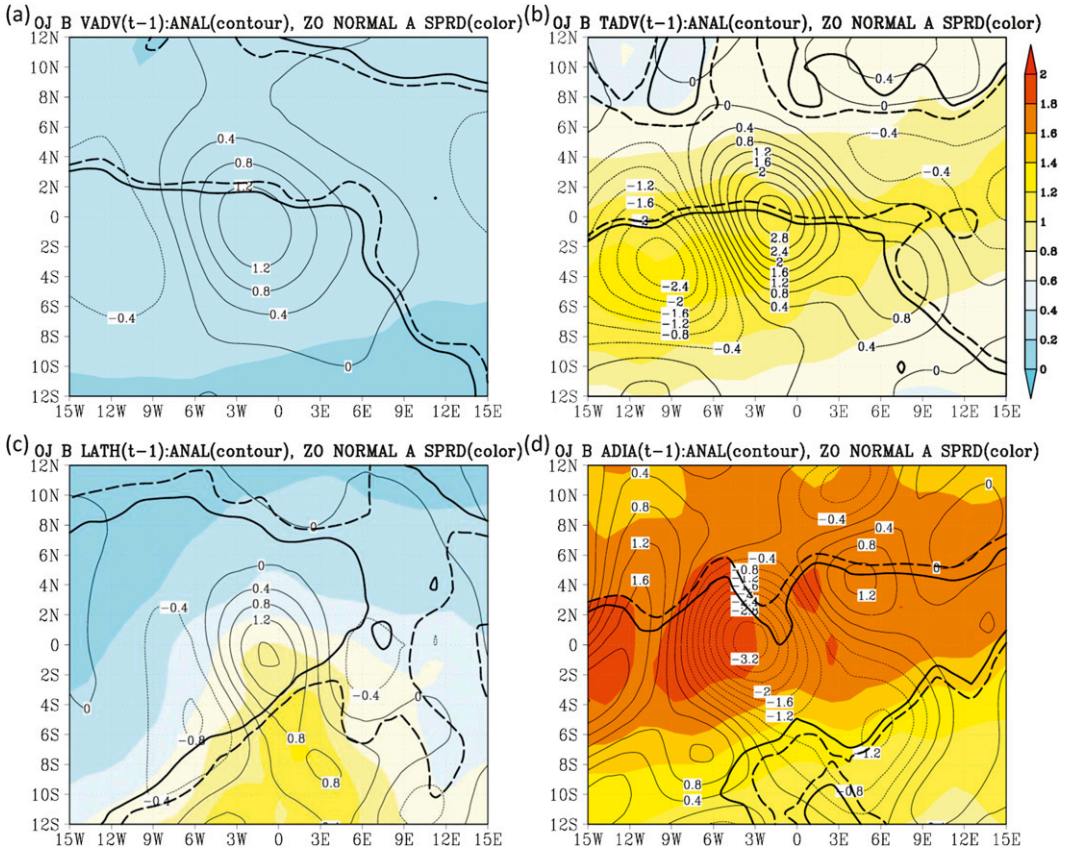

FIG. 11. As in Fig. 10, but for analysis spreads normalized by local standard deviations of the sum of the Z-O equation terms for time.

of the cyclone (Fig. 11d), and the TADV spread also shows a relatively large contribution southwest of the cyclone (Fig. 11b). The large spread of the ADIA appears between the positive and negative ADIA. Because the ADIA represents adiabatic warming associated with vertical motion, the spread implies an uncertainty of vertical motion around the tropopause fold. These results suggest that the source of the uncertainty is vertical motion at upper levels rather than the horizontal advections of vorticity and temperature for OJ B cyclones.

For PO A cyclones, the LATH spread shows a peak around the cyclone center and overlaps its positive contribution to the vorticity tendency with high significance (Fig. 12c). The TADV, VADV, and ADIA spreads of PO A cyclones are weaker than those of OJ B cyclones and their significance is low (Figs. 12a,b,d). It is notable that ADIA does not show a significant difference (Fig. 12d), although it shows a large signal that is the same as the LATH in increment analysis (Fig. 7d). This result suggests that the adiabatic warming error is not sensitive to an initial condition uncertainty, although its forecast fails in AFES. Thus, an improvement of vertical motion in the model will lead to more accurate prediction of PO A cyclones through adiabatic warming. This characteristic clearly appears in other spreads that are normalized by the sum of Z-O terms (Fig. 13). The VADV spread is smallest among the terms, and the TADV spread is similar to the small size of the spread of OJ B cyclones (Figs. 13a,b). It is notable that the spreads of VADV, TADV, and ADIA do not show a significant difference, which is different from OJ B cyclones (Figs. 13a,b,d). However, the LATH spread is large relative to the other terms, with high significance (Fig. 13c). These results indicate that diabatic heating by condensation is sensitive to initial condition error, which causes substantial uncertainty around the cyclone center in the prediction of PO A cyclones. Conversely the upper trough and temperature advection are relatively insensitive to initial condition uncertainty. These results suggest that additional observations around the cyclone center and the southwestern quadrant would help to improve PO A cyclone prediction.

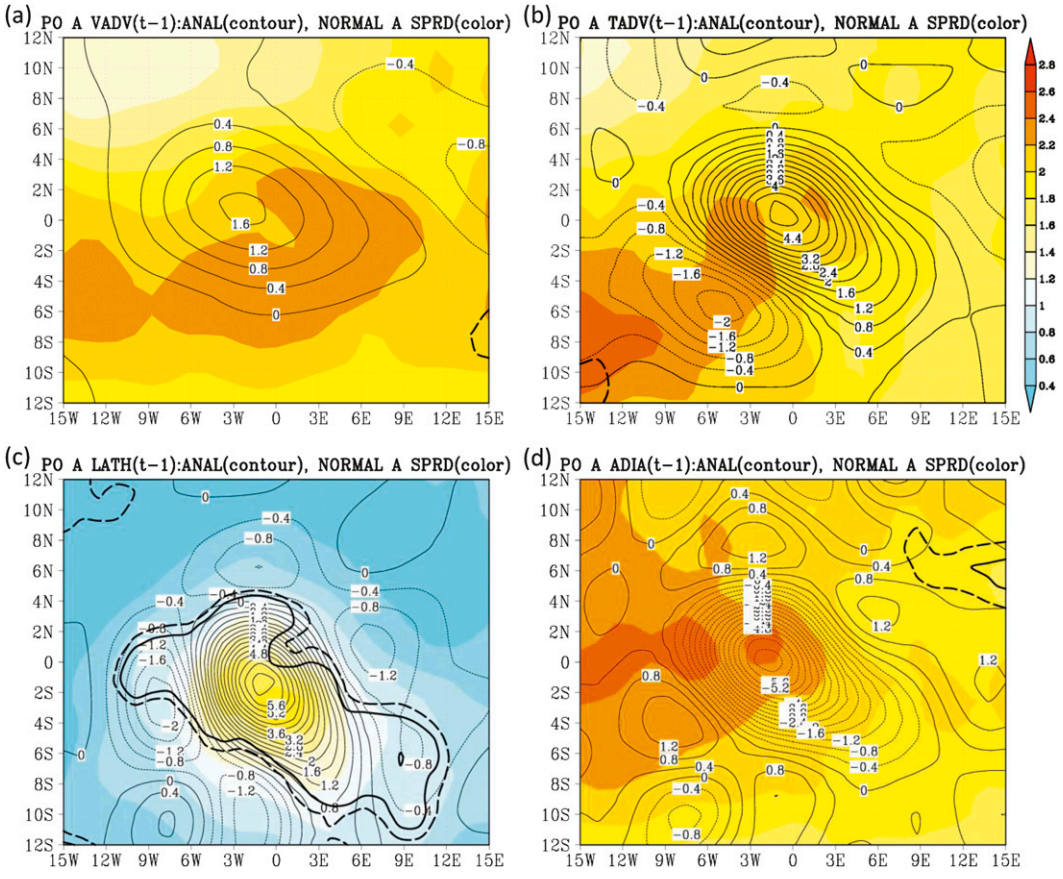

FIG. 12. As in Fig. 10, but for PO A cyclones.

4. Summary and conclusions

A predictability analysis of explosively developing extratropical cyclones (explosive cyclones) is undertaken using an ensemble reanalysis, ALERA. This dataset enables the estimation of analysis error and initial condition uncertainty using the increments and ensemble spreads, respectively. Cyclone-relative composite analyses of the increments and the ensemble spreads show that cyclone development mechanisms affect error growth and distribution. The first guess of OJ B cyclones that develop mainly as a result of vorticity advection places the cyclone north of the analyzed cyclone position. The forecast error is related to the adiabatic warming error associated with the vertical motion accompanying tropopause folding because of an upper trough position or depth error. The ensemble spread of the SLP is large to the west and southwest of the cyclone, whereas the spreads of geopotential height and temperature are large in the midtroposphere. The spread is also primarily associated with adiabatic warming accompanying the upper trough. These results suggest that the initial condition error around an upper trough associated with a tropopause folding significantly affects the predictability of OJ B cyclones.

Conversely, PO A cyclones developing as a result of latent heat release show higher central and southern SLP in the first guess than in the analysis. The underestimation of latent heat release around the cyclone center causes this error. The SLP spread is also large around the cyclone center because of the uncertainty of the latent heat release. Thus, the geopotential height and temperature spreads extend vertically over the cyclone center. The vertical distribution corresponds to the strong updraft associated with cloud condensation over the cyclone center of PO A cyclones (Kuwano-Yoshida and Asuma 2008), which suggests that latent heat release is important for the accurate prediction of PO A cyclones in addition to their explosive development. It may be reasonable that the error of latent heat release tends to be large because latent heat release error is the integrated result of the errors of moisture, wind, and temperature prediction. However, these results suggest that the large effect of latent heat release

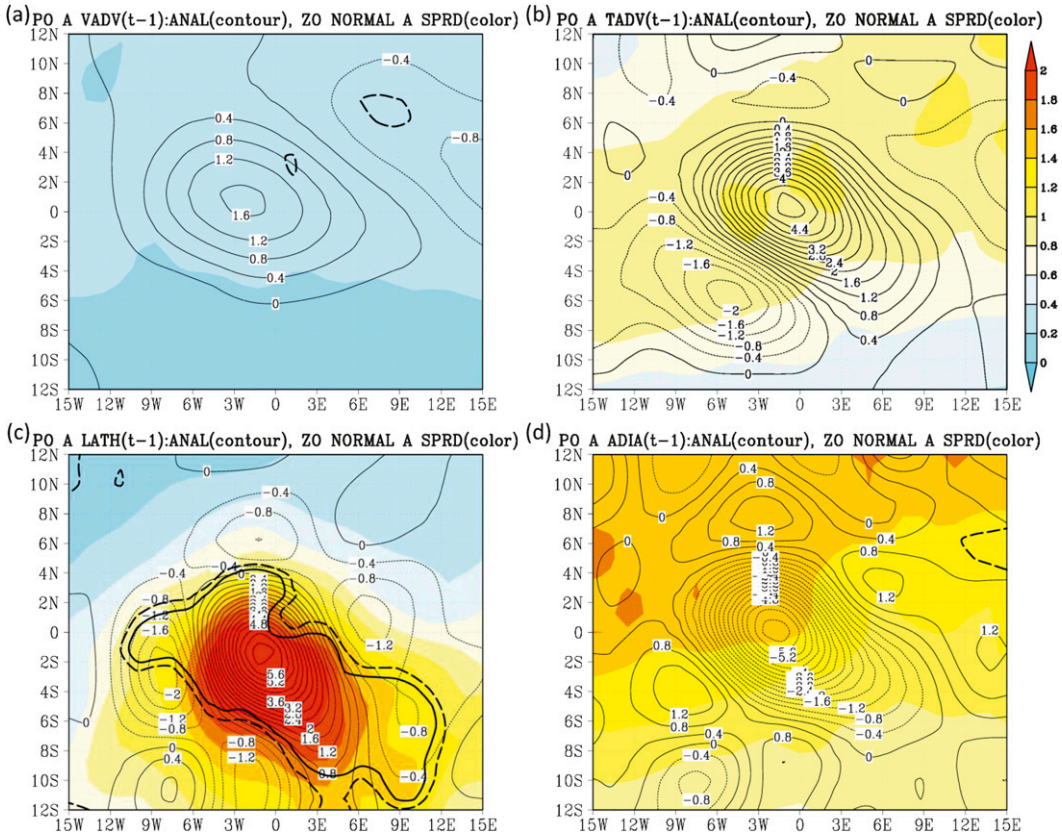

FIG. 13. As in Fig. 11, but for PO A cyclones.

on explosive cyclogenesis error is caused by the strong physical relationship between latent heat release and the explosive development of PO A cyclones. In addition, the increment and spread characteristics are not significant for weaker cyclogenesis both in OJ and PO cyclones. The results may suggest that large increment and spread are associated with extreme events that may break capacities and assumptions of model, observation, and data assimilation. Moreover, the cumulus and grid-scale condensation parameter settings used in AFES may increase this error because AFES has a precipitation bias in the tropics (Enomoto et al. 2008). This result also suggests that horizontal resolution is a factor in improving the prediction accuracy for explosive cyclogenesis. The 80-km grid spacing of AFES in ALERA is too coarse to represent the sharp ascending motion associated with cumulus convection within an explosive cyclone center. The results presented here demonstrate that the spatial structure of the model and initial value errors are associated with dominant processes in phenomena such as explosive cyclones. Because the results in the present study are obtained only from a single analysis system (ALERA), further examination of other analysis systems is required to confirm the consistency of our results with multiple models and data assimilation systems.

Our analysis suggests that further observation of the statistical target area around cyclones is required to improve the 6-h forecast of explosive cyclones. This information may be useful for targeting additional observations without relying on real-time sensitivity analysis. Experimental targeted observations based on real-time operational model forecast error information were gathered during in T-PARC for typhoons (Chou et al. 2011). However, conducting target observations for short range forecasts in real time is difficult because the time required for the sensitivity analysis limits the amount of lead time. In addition, the longer guidance time for target observations differs across analysis systems (Wu et al. 2009). Currently, ALERA2 has been constructed (Enomoto et al. 2013) to include the winter T-PARC data. Experiments using this system are ongoing and will provide greater clarity regarding the predictability and error structures of extratropical cyclones. In addition, higher-resolution models with nonhydrostatic equation sets may be required for more accurate forecasting of explosive cyclones.

Acknowledgments. AFES and ALERA are computed by the Earth Simulator supported by JAMSTEC. The authors appreciate N. Komori for his comments and suggestions to improve the manuscript. This work was supported by JSPS KAKENHI Grant-in-Aid for Young Scientists (B) (21740348).

REFERENCES

Blender, R., and M. Schubert, 2000: Cyclone tracking in different spatial and temporal resolutions. *Mon. Wea. Rev.,* **128,** 377–384.

Chen, S.-J., and L. Dell'osso, 1987: A numerical case study of East Asian coastal cyclogenesis. *Mon. Wea. Rev.,* **115,** 477–487.

——, Y.-H. Kuo, P.-Z. Zhang, and Q.-F. Bai, 1992: Climatology of explosive cyclones off the East Asian coast. *Mon. Wea. Rev.,* **120,** 3029–3035.

Chou, K.-H., C.-C. Wu, P.-H. Lin, S. D. Aberson, M. Weissmann, F. Harnisch, and T. Nakazawa, 2011: The impact of dropwindsonde observations on typhoon track forecasts in DOTSTAR and T-PARC. *Mon. Wea. Rev.,* **139,** 1728–1743.

Edmon, H. J., Jr., and D. G. Vincent, 1976: An application of two tropical parameterization schemes of convective latent heat release in middle latitudes. *Mon. Wea. Rev.,* **104,** 1141–1153.

Enomoto, T., A. Kuwano-Yoshida, N. Komori, and W. Ohfuchi, 2008: Description of AFES 2: Improvements for high-resolution and coupled simulations. *High Resolution Numerical Modelling of the Atmosphere and Ocean,* K. Hamilton and W. Ohfuchi, Eds., Springer, 77–97.

——, T. Miyoshi, Q. Moteki, J. Inoue, M. Hattori, A. Kuwano-Yoshida, N. Komori, and S. Yamane, 2013: Observing system research and ensemble data assimilation at JAMSTEC. *Data Assimilation for Atmospheric, Oceanic and Hydrologic Applications II,* S. K. Park and L. Xu, Eds., Springer, 509–526.

Froude, L. S. R., 2009: Regional differences in the prediction of extratropical cyclones by the ECMWF ensemble prediction system. *Mon. Wea. Rev.,* **137,** 893–911.

——, 2010: TIGGE: Comparison of the prediction of Northern Hemisphere extratropical cyclones by different ensemble prediction systems. *Wea. Forecasting,* **25,** 819–836.

——, 2011: TIGGE: Comparison of the prediction of Southern Hemisphere extratropical cyclones by different ensemble prediction systems. *Wea. Forecasting,* **26,** 388–398.

——, L. Bengtsson, and K. I. Hodges, 2007a: The predictability of extratropical storm tracks and the sensitivity of their prediction to the observing system. *Mon. Wea. Rev.,* **135,** 315–333.

——, ——, and ——, 2007b: The prediction of extratropical storm tracks by the ECMWF and NCEP ensemble prediction systems. *Mon. Wea. Rev.,* **135,** 2545–2567.

Gyakum, J. R., and Coauthors, 1996: A regional model intercomparison using a case of explosive oceanic cyclogenesis. *Wea. Forecasting,* **11,** 521–543.

Harr, P. A., R. L. Elsberry, T. F. Hogan, and W. M. Clune, 1992: Forecasts of North Pacific maritime cyclones with the Navy Operational Global Atmospheric Prediction System. *Wea. Forecasting,* **7,** 456–467.

Houtekamer, P. L., H. L. Mitchell, G. Pellerin, M. Buehner, M. Charron, L. Spacek, and B. Hansen, 2005: Atmospheric data assimilation with an ensemble Kalman filter: Results with real observations. *Mon. Wea. Rev.,* **133,** 604–620.

Koppel, L. L., L. F. Bosart, and D. Keyser, 2000: A 25-yr climatology of large-amplitude hourly surface pressure changes over the conterminous United States. *Mon. Wea. Rev.,* **128,** 51–68.

Krishnamurti, T. N., and W. J. Moxim, 1971: On parameterization of convective and nonconvective latent heat release. *J. Appl. Meteor.,* **10,** 3–13.

Kunii, M., and T. Miyoshi, 2012: Including uncertainties of sea surface temperature in an ensemble Kalman filter: A case study of Typhoon Sinlaku (2008). *Wea. Forecasting,* **27,** 1586–1597.

Kuo, H. L., 1965: On formation and intensification of tropical cyclone through latent heat release by cumulus convection. *J. Atmos. Sci.,* **22,** 40–63.

——, 1974: Further studies of the parameterization of the influence of cumulus convection on a large-scale flow. *J. Atmos. Sci.,* **31,** 1232–1240.

Kuo, Y.-H., and S. Low-Nam, 1990: Prediction of nine explosive cyclones over the western Atlantic Ocean with a regional model. *Mon. Wea. Rev.,* **118,** 3–25.

Kuwano-Yoshida, A., and Y. Asuma, 2008: Numerical study of explosively developing extratropical cyclones in the northwestern Pacific region. *Mon. Wea. Rev.,* **136,** 712–740.

Lin, S. C., and P. J. Smith, 1979: Diabatic heating and generation of available potential energy in a tornado-producing extratropical cyclone. *Mon. Wea. Rev.,* **107,** 1169–1183.

Lupo, A., P. Smith, and P. Zwack, 1992: A diagnosis of the explosive development of two extratropical cyclones. *Mon. Wea. Rev.,* **120,** 1490–1523.

Majumdar, S. J., K. J. Sellwood, D. Hodyss, Z. Toth, and Y. Song, 2010: Characteristics of target areas selected by the ensemble transform Kalman filter for medium-range forecasts of high-impact winter weather. *Mon. Wea. Rev.,* **138,** 2803–2824.

Miyoshi, T., and S. Yamane, 2007: Local ensemble transform Kalman filtering with an AGCM at a T159/L48 resolution. *Mon. Wea. Rev.,* **135,** 3841–3861.

——, ——, and T. Enomoto, 2007: The AFES-LETKF experimental ensemble reanalysis: ALERA. *SOLA,* **3,** 45–48.

Moteki, Q., and Coauthors, 2011: The influence of observations propagated by convectively coupled equatorial waves. *Quart. J. Roy. Meteor. Soc.,* **137** (656), 641–655.

Nuss, W. A., and S. I. Kamikawa, 1990: Dynamics and boundary layer processes in two Asian cyclones. *Mon. Wea. Rev.,* **118,** 755–771.

O'Brien, J. J., 1970: Alternative solutions to the classical vertical velocity problem. *J. Appl. Meteor.,* **9,** 197–203.

Ohfuchi, W., and Coauthors, 2004: 10-km mesh meso-scale resolving simulations of the global atmosphere on the Earth Simulator: Preliminary outcomes of AFES (AGCM for the Earth Simulator). *J. Earth Simulator,* **1,** 8–34.

Roebber, P. J., 1984: Statistical analysis and updated climatology of explosive cyclones. *Mon. Wea. Rev.,* **112,** 1577–1589.

——, and M. R. Schumann, 2011: Physical processes governing the rapid deepening tail of maritime cyclogenesis. *Mon. Wea. Rev.,* **139,** 2776–2789.

Sanders, F., 1987: Skill of NMC operational dynamical models in prediction of explosive cyclogenesis. *Wea. Forecasting,* **2,** 322–336.

——, and J. R. Gyakum, 1980: Synoptic-dynamic climatology of the "bomb." *Mon. Wea. Rev.,* **108,** 1589–1606.

——, S. L. Mullen, and D. P. Baumhefner, 2000: Ensemble simulations of explosive cyclogenesis at ranges of 2–5 days. *Mon. Wea. Rev.,* **128,** 2920–2934.

Shapiro, M., and Coauthors, 1999: A planetary-scale to mesoscale perspective of the life cycles of extratropical cyclones: The

bridge between theory and observations. *The Life Cycles of Extratropical Cyclones,* M. Shapiro and S. Gronas, Eds., Amer. Meteor. Soc., 139–186.

——, and Coauthors, 2010: An earth-system prediction initiative for the twenty-first century. *Bull. Amer. Meteor. Soc.,* **91,** 1377–1388.

Shapiro, R., 1970: Smoothing, filtering, and boundary effects. *Rev. Geophys. Space Phys.,* **8,** 359–387.

Smith, P. J., P. M. Dare, and S.-J. Lin, 1984: The impact of latent heat release on synoptic scale vertical motions and development of an extratropical cyclone system. *Mon. Wea. Rev.,* **112,** 2421–2430.

Tilly, D. E., A. R. Lupo, C. J. Melick, and P. S. Market, 2008: Calculated height tendencies in two Southern Hemisphere blocking and cyclone events: The contribution of diabatic heating to block intensification. *Mon. Wea. Rev.,* **136,** 3568–3578.

Uccellini, L. W., D. Keyser, K. F. Brill, and C. H. Wash, 1985: The Presidents' Day Cyclone of 18–19 February 1979: Influence of upstream trough amplification and associated tropopause folding on rapid cyclogenesis. *Mon. Wea. Rev.,* **113,** 962–988.

——, R. A. Petersen, P. J. Kocin, K. F. Brill, and J. J. Tuccillo, 1987: Synergistic interactions between an upper-level jet streak and diabatic processes that influence the development of a low-level jet and a secondary coastal cyclone. *Mon. Wea. Rev.,* **115,** 2227–2261.

Vincent, D. G., G. B. Pant, and H. J. Edmon Jr., 1977: Generation of available potential energy of an extratropical cyclone system. *Mon. Wea. Rev.,* **105,** 1252–1265.

Wu, C.-C., and Coauthors, 2009: Intercomparison of targeted observation guidance for tropical cyclones in the northwestern Pacific. *Mon. Wea. Rev.,* **137,** 2471–2492.

Yoshida, A., and Y. Asuma, 2004: Structures and environment of explosively developing extratropical cyclones in the northwestern Pacific region. *Mon. Wea. Rev.,* **132,** 1121–1142.

Zhang, F., 2005: Dynamics and structure of mesoscale error covariance of a winter cyclone estimated through short-range ensemble forecasts. *Mon. Wea. Rev.,* **133,** 2876–2893.

Zwack, P., and B. Okossi, 1986: A new method for solving the quasi-geostrophic omega equation by incorporating surface pressure tendency data. *Mon. Wea. Rev.,* **114,** 655–666.